



## Dynamic failure of the aluminium plate under air-blast loading in the framework of the fractional viscoplasticity model - theory and validation

Wojciech Sumelka<sup>\*,a</sup>, Marcin Nowak<sup>b</sup>, Amr A. Nassr<sup>c</sup>, Hasan Al-Rifaie<sup>a</sup>, Michał Malendowski<sup>a</sup>, Tomasz Gajewski<sup>a</sup>, Piotr Peksa<sup>a</sup>, Robert Studziński<sup>d</sup>, Piotr W. Sielicki<sup>a</sup>

<sup>a</sup> Poznan University of Technology, Institute of Structural Analysis, Poland

<sup>b</sup> Institute of Fundamental Technological Research Polish Academy of Sciences, Poland

<sup>c</sup> Department of Civil Engineering, Assiut University, Assiut, 71111, Egypt

<sup>d</sup> Poznan University of Technology, Institute of Building Engineering, Poland

### ARTICLE INFO

#### Keywords:

Fractional viscoplasticity  
Rate sensitivity  
Plastic anisotropy  
Non-locality  
Damage mechanics

### ABSTRACT

This paper deals with the numerical simulation of the dynamic failure of an aluminium plate under air-blast loading. Constitutive modelling based on the fractional viscoplasticity is used. The material model is non-local due to the properties of the applied fractional differential operator and is implemented as user material in the engineering finite element computation code ABAQUS. It is important that the numerical simulations are contrasted with experiments. Numerical outcomes clearly show the applicability of the adopted modelling for the description of salient stages of dynamic structural failure.

### 1. Introduction

Over the last decade, protection of civilians, military and industrial structures against impact and blast loading has received a lot of attention (Hanssen et al. [12], Brovik et al. [5,6], Grimsmo et al. [10], Aune et al. [4]). Such structures are often made of different materials depending on the intended use. Herein, the masonry or concrete walls as supporting walls for buildings and temporary fast-build shelters (Sielicki and Lodygowski [36], Clarke et al. [8], Kuczewicz et al. [16], Sielicki et al. [37]), bullet- and blast-proves windows (Sielicki et al. [34], Zhang et al. [52]) or typical steel columns supporting a long-span ceiling at the public infrastructure (Sielicki et al. [35], Denny et al. [9], Sabuwala et al. [32], Hadianfard et al. [11]) are the most popular in the area of protective structures. Nonetheless, recently, the designers use also other important structural elements which are made on steel plates due to their superior properties including high strength, high ductility and good formability (Al-Rifaie and Sumelka [2], Neuberger et al. [21], Rigby et al. [31]). Plates, especially thin plates, are frequently being used as major components in engineering structures, thus it has become necessary to evaluate the structural response of such components exposed to blast loading. Nurick and Martin [23,24] presented a comprehensive literature review of thin plates subjected to blast loading. These studies included theoretical considerations, experimental

techniques, and experimental results for relatively large permanent displacements. Olson et al. [25] and Teeling-Smith and Nurick [48] studied the failure modes on steel plates subjected to blast and impulsive loading, they identified three different failure modes, i.e., large inelastic deformation (mode I), tensile tearing at supports (mode II) and transverse shear at supports (mode III). Subsequent work by Nurick et al. [22] extended these failure modes by including necking at the boundary for mode I, and some geometric additions to mode II by including the amount of tearing at the boundary (called mode II\* in the literature) - hence the experimental evidence was used to show a significant effect of the boundary conditions when predicting tearing. Similar results were also reported by Wierzbicki and Nurick [50]. Concluding, many experimental and numerical studies are available in literature aiming to reproduce the damage of a plate under low to moderate air-blast loading induced energy, see e.g. [3,19,30]. However, works regarding numerical modelling attempting to describe all the air-blast post-loaded states, i.e. plasticity spreading, are scarce.

Based on the above statements, a material model that can simulate the mechanical response of the physical target under the blast loading is desired. Herein, the fractional calculus which has been used to study a lot of problems in physics including diffusion, fluid flow, statistics, viscoelasticity, rheology, electrochemistry of corrosion, optics, and other [14,17,20,27,33,47,51] can extend classical formulations. As

\* Corresponding author.

E-mail address: [wojciech.sumelka@put.poznan.pl](mailto:wojciech.sumelka@put.poznan.pl) (W. Sumelka).

<https://doi.org/10.1016/j.ijimpeng.2021.104024>

Received 3 January 2021; Received in revised form 25 August 2021; Accepted 3 September 2021

Available online 10 September 2021

0734-743X/© 2021 The Author(s).

Published by Elsevier Ltd.

This is an open access article under the CC BY-NC-ND license

(<http://creativecommons.org/licenses/by-nc-nd/4.0/>).

presented by Sumelka [42], in the framework of space-fractional model, the application of fractional derivative in plasticity can be successful and furthermore in the framework of stress-fractional models cf. Szymczyk et al. [46], Sumelka et al. [40] and others [18,29,38,43] many engineering problems can be mapped with high precision. All the above results prompted the authors of this study to validate the stress-fractional viscoplasticity model defined in Szymczyk et al. [45], for dynamic failure of the aluminium plate under air-blast loading.

The next parts of this work aim at reporting numerical analysis and experimental validation of failure mechanisms of an aluminium plate subjected to air-blast loading presented in Aune et al. [3]. As mentioned the stress-fractional viscoplasticity non-local model Szymczyk et al. [45] is used as a constitutive law. The constitutive equations are implemented as user material in the engineering finite element computation code ABAQUS [1]. The modelling assumes adiabatic conditions including isotropic work hardening-softening effects induced by plastic strains, temperature and damage (scalar). Moreover, thin plate anisotropy induced by plastic strain evolution as well as rate-dependence are taken into account also.

The paper is structured as follows. Section 2 describes stress-fractional viscoplasticity model (sFVM). Section 3 reports the identification of sFVM parameters for aluminium alloy EN AW 1050A-H14 type. Section 4 discuss the numerical model for modelling failure mechanisms of an aluminium plate subjected to air-blast loading. In Section 5 the comparison of numerical and experimental results is presented. Finally, Section 6 concludes the paper.

## 2. Stress-fractional viscoplasticity - adiabatic conditions

Fractional viscoplasticity model and its implementation in the framework of the Finite Element Method (FEM) has been extensively described in the literature [39,45,46]. The main concept in this model lays in the fact that the classical Perzyna viscoplasticity model [26] is generalised utilising fractional calculus [13,28]. Namely, assuming standard total strain decomposition into elastic and plastic parts

$$\dot{\boldsymbol{\varepsilon}} = \dot{\boldsymbol{\varepsilon}}^e + \dot{\boldsymbol{\varepsilon}}^p, \quad (1)$$

with elastic part governed by Hooke's law

$$\boldsymbol{\sigma}^e = \mathcal{L}^e : \dot{\boldsymbol{\varepsilon}}^e, \quad (2)$$

we postulate the evolution of plastic part in a form

$$\dot{\boldsymbol{\varepsilon}}^p = \Lambda \mathbf{p}, \quad (3)$$

where the direction of flow  $\mathbf{p}$  is computed utilising Riesz-Caputo (RC) fractional derivative, namely

$$\mathbf{p} = D_{\sigma}^{\alpha} F. \quad (4)$$

In above  $\boldsymbol{\varepsilon}$  stands for total second order strain tensor,  $\boldsymbol{\varepsilon}^e$  and  $\boldsymbol{\varepsilon}^p$  denote elastic and plastic strains,  $\boldsymbol{\sigma}^e$  denotes the second order Cauchy stress tensor,  $\mathcal{L}^e$  denotes the fourth order elastic constitutive tensor,  $\Lambda$  is a scalar multiplier,  $F$  is the yield function,  $D_{\sigma}^{\alpha}$  denotes partial fractional differentiation of RC type, and  $\alpha$  denotes the order of derivative (the order of flow). It is important that for  $\alpha = 1$  a smooth passage to the classical associated plastic flow is obtained.

By analogy to [41] the flow vector  $\mathbf{p}$  is expressed by the following formula

$$p_i = P_{ij} M_{ij}, \quad (5)$$

where  $M_{ij}$  matrix contains the values of the classical derivative of the yield function with respect to the component of the stress tensor ( $\sigma_i = (\sigma_{11}, \sigma_{22}, \sigma_{33}, \sigma_{12}, \sigma_{13}, \sigma_{23})$ ) therefore

$$M_{ij} = \frac{\partial f}{\partial \sigma_j} \Big|_{\sigma_j = X_{ij}}, \quad \text{for } i = (1, 2, \dots, n_p), \quad j = (1, 2, \dots, 6). \quad (6)$$

The dimension of matrix  $M_{ij}$  is  $(n_p, 6)$  where  $n_p = (m_a - 1) + (m_b - 1) + 3$ . Parameters  $m_a$  and  $m_b$  describe number of discretisation points used to map the virtual stress surrounding and  $X_{ij}$  is defined as follows:

$$\begin{aligned} \text{for } i = 1, & & X_{ij} &= \sigma_j - \Delta_j, \\ \text{for } i = (2, 3, \dots, m_a), & & X_{ij} &= \sigma_j + \left(\frac{i}{m_a} - 1\right) \Delta_j, \\ \text{for } i = m_a + 1, & & X_{ij} &= \sigma_j, \\ \text{for } i = (m_a + 2, m_a + 3, \dots, n_p - 1), & & X_{ij} &= \sigma_j + \frac{i - m_a}{m_b} \Delta_j, \\ \text{for } i = n_p, & & X_{ij} &= \sigma_j + \Delta_j, \end{aligned} \quad (7)$$

where  $\Delta = (\Delta_{11}, \Delta_{22}, \Delta_{33}, \Delta_{12}, \Delta_{13}, \Delta_{23})$ . It is important that  $\Delta$  contains material constants and should be interpreted as the offset of the actual stress state to the left,  $\sigma_{ij}^L = \sigma_{ij} - \Delta_{ij}$ , or to the right,  $\sigma_{ij}^R = \sigma_{ij} + \Delta_{ij}$ .

In the presented approach we accept the shear yield function definition in the following form

$$f = \sqrt{J_2 + J_1^2 \cdot (n_1(\vartheta) + n_2(\vartheta)\xi)} - \kappa = 0, \quad (8)$$

where  $J_1 = \sigma_{11} + \sigma_{22} + \sigma_{33}$  is the first invariant of Cauchy stress tensor  $\boldsymbol{\sigma}$  and  $J_2$  is the second invariant of the deviatoric part of Cauchy stress tensor  $\boldsymbol{\sigma}'$

$$J_2 = \sqrt{\sigma_{12}^2 + \sigma_{13}^2 + \sigma_{23}^2 + \frac{1}{6} \left( (\sigma_{11} - \sigma_{22})^2 + (\sigma_{22} - \sigma_{33})^2 + (\sigma_{33} - \sigma_{11})^2 \right)}. \quad (9)$$

Variables  $n_1(\vartheta)$ ,  $n_2(\vartheta)$  are material parameters which in the general case are functions of temperature  $\vartheta$  [49], whereas  $\xi$  is the scalar damage parameter ( $\xi \in [0, \xi_F]$  - where 0 means undamaged material and  $\xi_F$  means total loss of load carrying-capacity). Finally,  $\kappa$  is the shear yield stress.

For postulated scalar damage parameter we postulate the evolution law using the rate form

$$\dot{\xi}_{grow} = \frac{g^*(\xi, \vartheta)}{T_m \kappa_0(\vartheta)} < I_g - \tau_{eq}(\xi, \vartheta, \epsilon^p) >, \quad (10)$$

where:

$$g^*(\xi, \vartheta) = c_1(\vartheta) \frac{\xi}{1 - \xi},$$

$$I_g = b_1 J_1 + b_2 \sqrt{J_2},$$

$$\tau_{eq}(\xi, \vartheta, \epsilon^p) = c_2(\vartheta) (1 - \xi) \ln \frac{1}{\xi} \left\{ 2\kappa_s(\vartheta) - [\kappa_s(\vartheta) - \kappa_0(\vartheta)] F(\xi_0, \xi, \vartheta) \right\},$$

$$F(\xi_0, \xi, \vartheta) = \left( \frac{\xi_0}{1 - \xi_0} \frac{1 - \xi}{\xi} \right)^{(2/3)\delta(\vartheta)} + \left( \frac{1 - \xi}{1 - \xi_0} \right)^{(2/3)\delta(\vartheta)},$$

and  $b_1$ ,  $b_2$ ,  $c_1$ ,  $c_2$  and  $\xi_0$  are additional material parameters. Furthermore the isotropic work hardening-softening of the material takes the form

$$\kappa = \bar{\kappa} \left( \xi, \vartheta, \epsilon^p \right) = \left\{ \kappa_s(\vartheta) - [\kappa_s(\vartheta) - \kappa_0(\vartheta)] \exp[-\delta(\vartheta) \epsilon^p] \right\} \left[ 1 - \left( \frac{\xi}{\xi_F} \right)^{\beta(\vartheta)} \right], \quad (11)$$

where:

**Table 1**

Classical material parameters for the stress-fractional viscoplasticity model for aluminium alloy EN AW 1050A-H14 type.

$\kappa_s^* = 76$ MPa	$\kappa_s^{**} = 47$ MPa	$\kappa_0^* = 70$ MPa	$\kappa_0^{**} = 37$ MPa	$\delta^* = 28$
$\delta^{**} = 8$	$\beta^* = 2.2$	$\beta^{**} = 0.9$	$\vartheta_0 = 293$ K	$\xi_F = 0.8$
$\rho_{ref} = 2700$ kg/m <sup>3</sup>	$E = 70$ GPa	$\nu = 0.3$	$T_m = 0.01$ $\mu$ s	$m = 1$
$c_1 = 0.0006$	$c_2 = 0.07$	$b_1 = 1.0$	$b_2 = 1.3$	$\xi_0 = 6 \cdot 10^{-4}$
$n_1 = 0$	$n_2 = 0.25$	$\chi^* = 0.9$	$c_p = 910$ J/kg K	

**Table 2**

Fractional material parameters for the stress-fractional viscoplasticity model for aluminium alloy EN AW 1050A-H14 type.

$\alpha = 0.5$	$\Delta_{11}^{L,R} = 3.0$	$\Delta_{22}^{L,R} = 1.0$	$\Delta_{33}^{L,R} = 1.0$	$\Delta_{12}^{L,R} = 1.0$	$\Delta_{13}^{L,R} = 1.0$	$\Delta_{23}^{L,R} = 1.0$
----------------	---------------------------	---------------------------	---------------------------	---------------------------	---------------------------	---------------------------

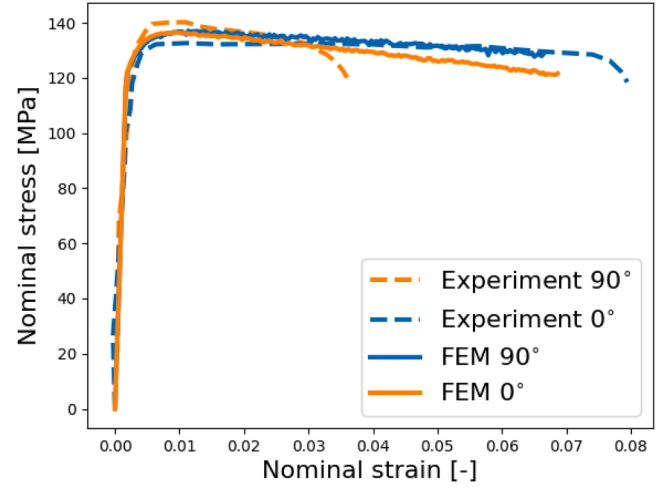


**Fig. 2.** Comparison of nominal stress vs nominal strain curve from numerical simulations and experimental data during uni-axial tension test of aluminium alloy EN AW 1050A-H14 type.

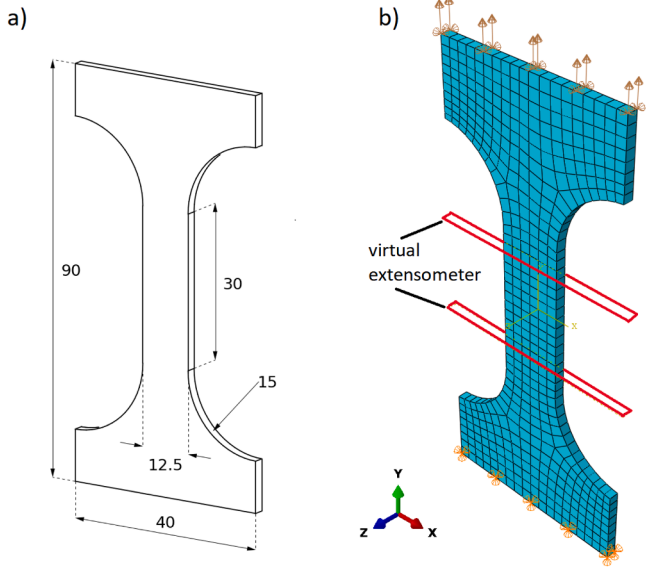


**Fig. 1.** a) Geometry of the test specimen (in mm) b) finite element model of uniaxial tension test.

$$\kappa_s(\vartheta) = \kappa_s^* - \kappa_s^{**} \bar{\vartheta},$$

$$\kappa_0(\vartheta) = \kappa_0^* - \kappa_0^{**} \bar{\vartheta},$$

$$\beta(\vartheta) = \beta^* - \beta^{**} \bar{\vartheta},$$

$$\bar{\vartheta} = \frac{\vartheta - \vartheta_0}{\vartheta_0}$$

$$\delta(\vartheta) = \delta^* - \delta^{**} \bar{\vartheta}.$$

and  $\kappa_0^{**}, \kappa_s^*, \kappa_s^{**}, \beta^*, \beta^{**}, \delta^*, \delta^{**}$  and  $\xi_F$  are material parameters. Parameter  $\vartheta_0$  is the reference temperature, equal to 293 K in our case.

Taking into account the above postulates, the evolution of temperature in the adiabatic regime has the form

$$\dot{\vartheta} = \frac{\chi^*}{\rho c_p} \sigma : \dot{\epsilon}^p + \frac{\chi^{**}}{\rho c_p} \dot{\xi}_{grow}, \quad (12)$$

where  $\rho$  is the density of the material, and  $c_p$  is specific heat. In following, we assume that  $\chi^{**} = 0$ , which means that the temperature is generated only by the part of the plastic work controlled solely by  $\chi^*$

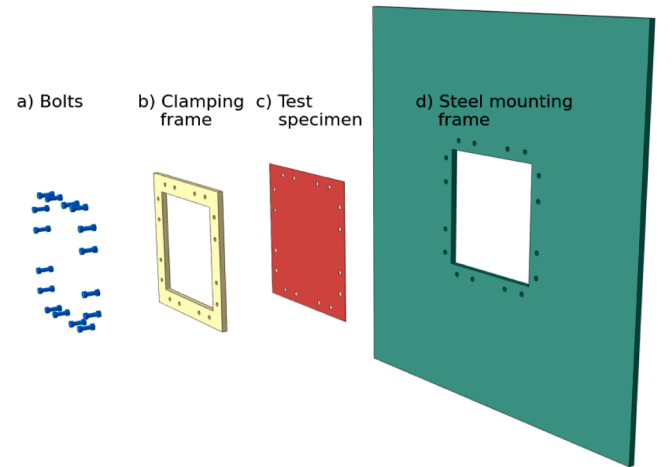


**Fig. 3.** Individual parts of the tested system. a) 16 tightened bolts, b) clamping frame for fixed boundary conditions, c) square plate specimens with dimensions of  $0.4m \times 0.4m \times 0.0008m$  and d) steel mounting frame with outer dimensions  $1.0m \times 1.0m \times 0.015m$  and a square opening of  $0.3m \times 0.3m$  in the centre.

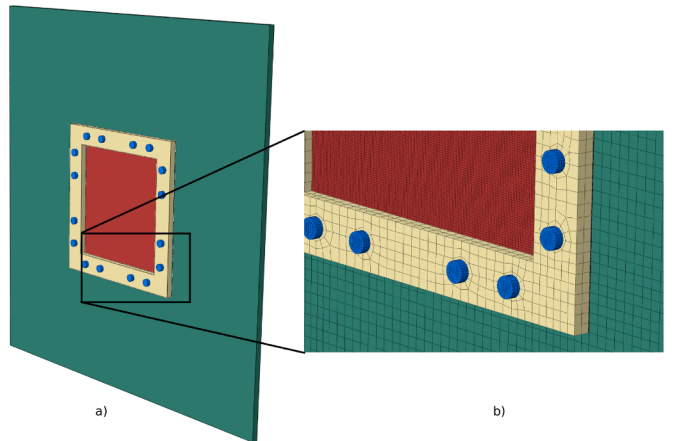


**Fig. 4.** a) Assembly of all parts for numerical simulations, b) view of a fragment of a finite element mesh.

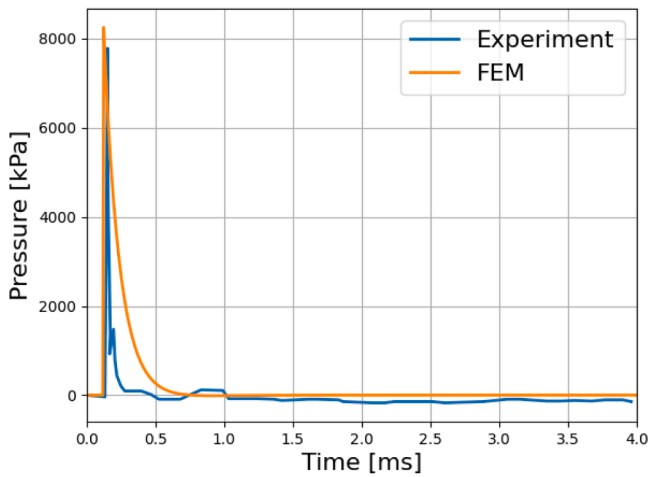


Fig. 5. Comparison of the overpressure history for point in the middle of the sample for 0.04kg TNT in 0.625m stand-off distance.

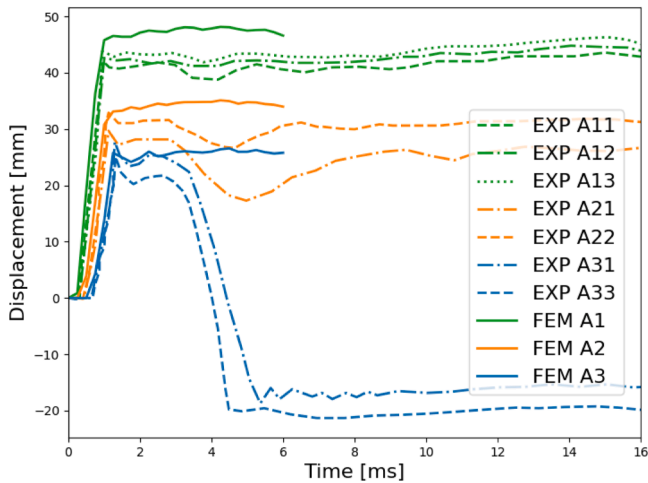


Fig. 6. Comparison of displacement history for the point in the middle of the plate. The charge-to-sample distances are equal to 0.375m for A11, A12, A13, 0.500m for A21, A22 and 0.625m for A31, A33.

[49].

To conclude, in the proposed constitutive model (assuming isotropic law in the elastic range) the total number of the material parameters is equal to 31 (cf. Table 1 and Table 2). Fractional material parameters (Table 2) dictate the dynamism of the whole process and results in high flexibility to mimic the experimental observations. In this sense, both parameters  $\Delta$  and  $\alpha$  control the level of induced plastic anisotropy. Increasing the value of selected  $\Delta_{ij}$  parameter causes the intensified viscoplastic flow in this direction (for more details see [45]) and change in the geometry of the plastic strain localization patterns and sensitivity to the rate of plastic strains. This in consequence finally modifies the evolution of the temperature, damage, and yield limit.

### 3. Identification

To calibrate the fractional viscoplastic model the experimental data of the uniaxial tension tests for aluminium alloy EN AW 1050A-H14 type were taken from [3]. In [3], the experimental investigation was performed on dogbone shape specimens with dimensions presented in Fig. 1 (a). The analysed samples were cut from a 2mm thick metal sheet which exhibits plastic anisotropy. Depending on the stretching direction (consistent with the rolling direction, perpendicular to the rolling

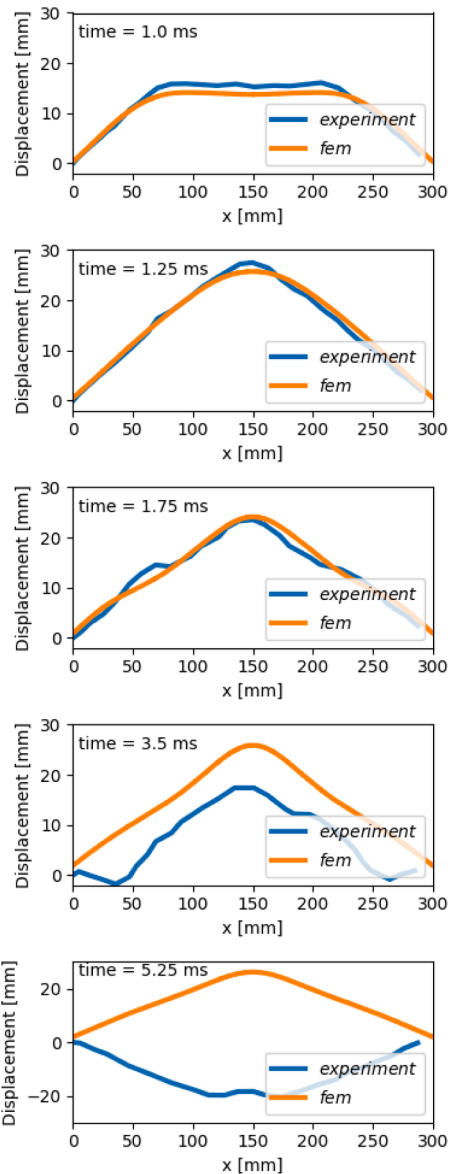


Fig. 7. Comparison of deformation profile at centre along x-axis for selected time instances - EXP A31 vs. FEM A3 - cf. Fig. 6.

direction or at 45° to the rolling direction) the different responses in terms of stress-strain curves were obtained.

The calibration procedure of the constitutive model consisted of carrying out a series of numerical simulations of the uniaxial tension test and comparing them with stress-strain curves from the experimental data. In Fig. 1b the finite element model of tension test is shown. The bottom plane of the sample was fixed. The velocity boundary condition (3mm/s) was applied to the top plane of the sample. The duration of the deformation process was set to 0.5s. Such conditions approximately correspond to a quasi-static process. For measuring averaged strains in the gauge section the virtual extensometer was defined Fig. 1(b).

The material parameters obtained as a result of fitting the stress-strain curves are given in Tabs 1, 2.

In Fig. 2 the response from the calibrated fractional model is confronted against the results from experiments. A good agreement of the results is observed, especially for direction 90° which is perpendicular to the rolling direction of the analysed for aluminium alloy sheet.

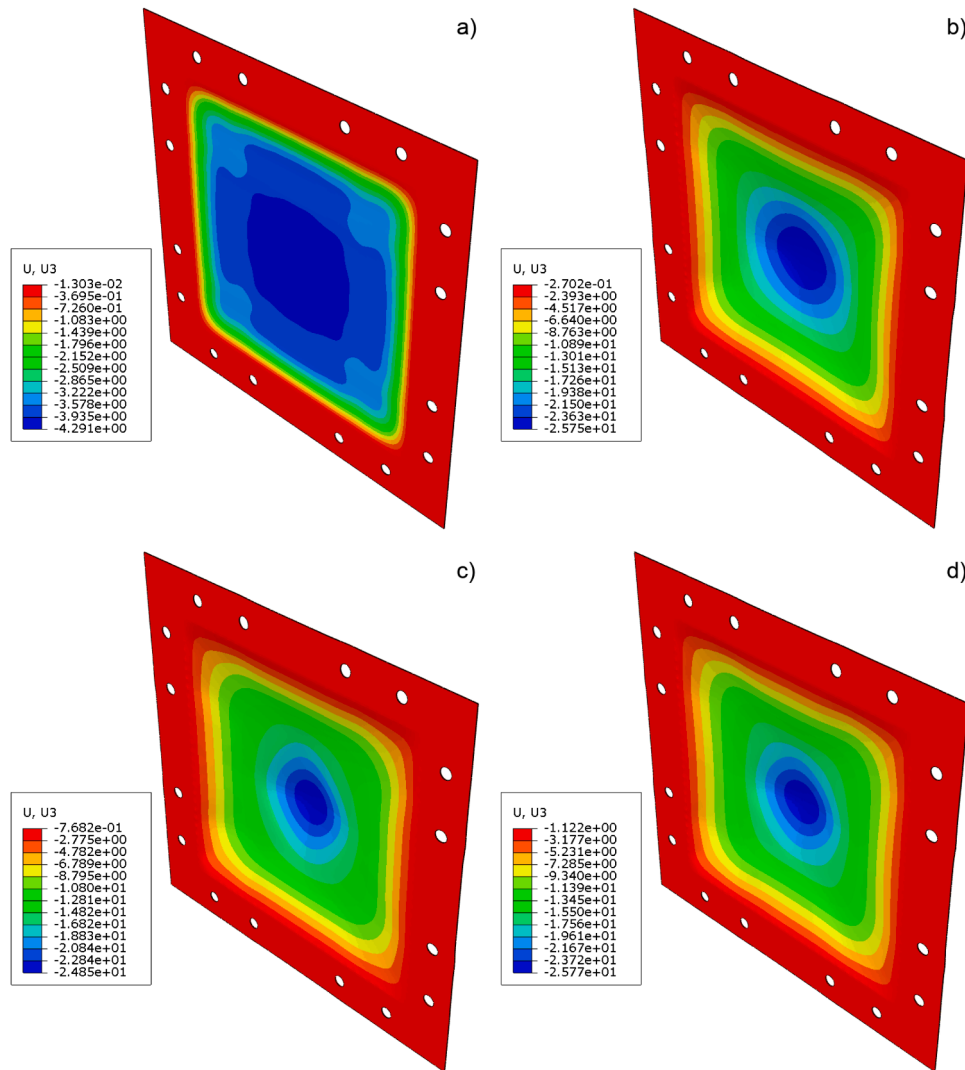


Fig. 8. Evolution of out of plane component of displacement vector for time instances a) 0.25ms, 1.25ms, c) 3.0ms and d) 6.0ms.

## 4. Experiment description and computational model

### 4.1. Experimental data

All experimental data presented in this section were taken from the work [3]. The experiment aimed to measure the displacement field of thin aluminium sheets subjected to air blast loading. The displacement measurement was performed using the digital image correlation method (DIC 3D) based on the registered images from two high-speed cameras in a stereoscopic setup. Pressure measurements at various locations were made using piezoelectric pressure sensors. Three stand-off distances of the explosive mass were analyzed: 0.375 (marked as A1), 0.500 (marked as A2) and 0.625 (marked as A3). The explosive mass had a spherical shape with an approximate diameter equal to 34.5mm and a mass of 30g, which is equivalent to 40.2g of TNT.

### 4.2. Finite element model

The finite element model of testing system was created using the ABAQUS/CAE software. The model consists of 4 main parts which are presented in Fig. 3. The square aluminium sheet (c) with dimensions of  $0.4m \times 0.4m \times 0.0008m$  which is clamped to the steel mounting frame (d) using clamping frame (b) and bolts (a). The 16 bolts were used to tighten the specimen to the mounting frame. The final assembly of these

parts is shown in Fig 4(a). The whole finite element (FE) model was discretized using C3D8 elements (eight-node linear brick element). A certain part of the finite element mesh is shown in Fig. 4(b). The total number of nodes and elements is 214584 and 278623, respectively. The corners of the mounting plate were fixed by prescribing displacement boundary condition equal to 0 (this simplification compared to data in [3] was dictated by the lack of data - it will have decisive meaning for selected configuration of blast loading). Finally, the air-blast loading modelled utilising the \*CONWEP CHARGE PROPERTY option with the following parameters: equivalent mass of TNT -  $4.02 \cdot 10^{-5}$  tone and multiplication factor equal to 1000.

As mentioned, the material model of aluminium presented in Section 2 was implemented through a VUMAT user subroutine. A detailed description of the finite element implementation of the fractional model can be found in [45]. Moreover the parts (a), (b) and (d) were modelled as isotropic elastic material with following material parameters: Young modulus 210 GPa, Poisson ratio 0.33, and density  $7850 \text{ kg/m}^3$ . The overall model was calculated in the Abaqus/Explicit program. The process time was set to 6ms.

## 5. Discussion

The calibrated fractional viscoplastic constitutive model (Section 3) was used to perform numerical analysis of the dynamic failure of

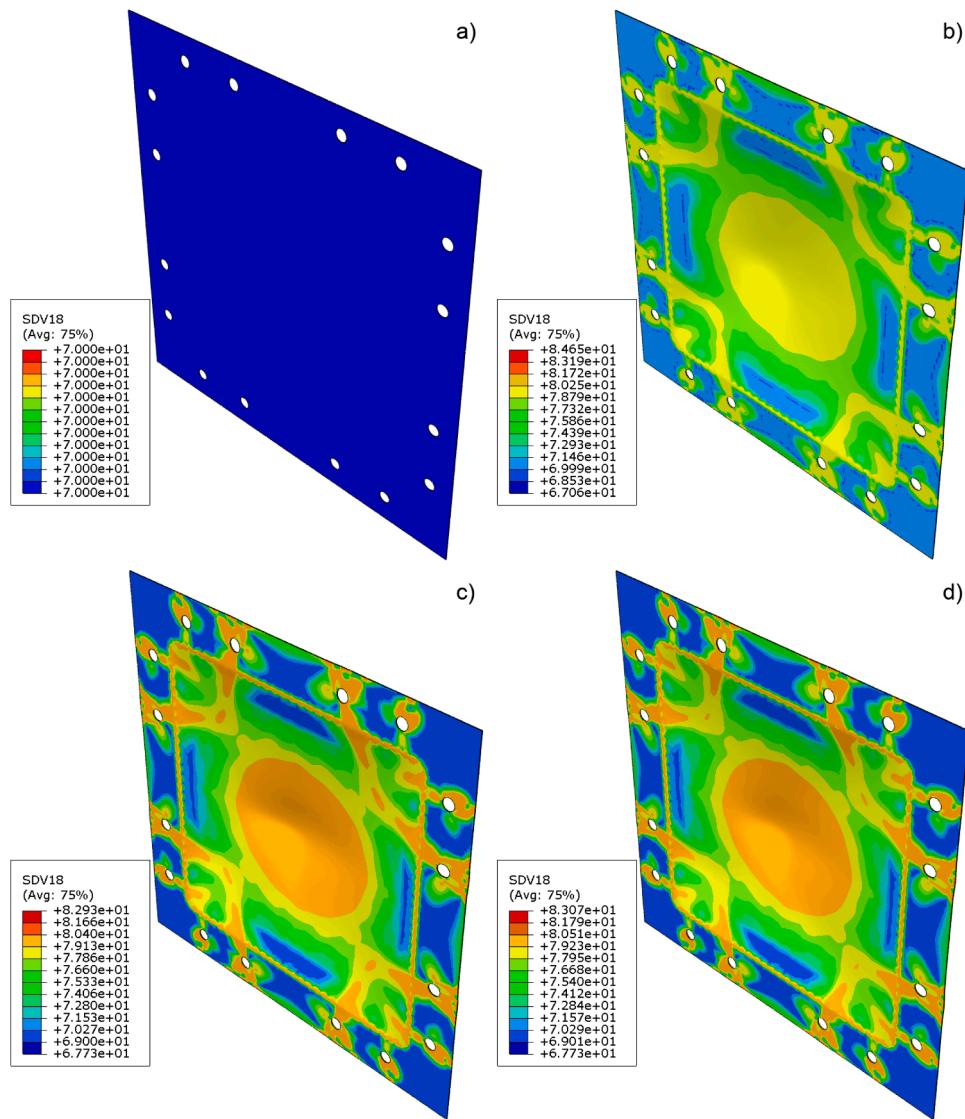


Fig. 9. Evolution of dynamic plastic yield stress for time instances a) 0.25ms, 1.25ms, c) 3.0ms and d) 6.0ms.

aluminium plate under air-blast loading presented in [3]. In the first step, it was checked whether the pressure loading model gives an acceptable effect. For this purpose, the history of pressure on the surface in the middle point was compared Fig. 5. Although the presented curves do not match exactly, the maximum pressure level is almost the same. After the observed peak value, the pressure drops and fluctuates around zero.

During the deformation process, the plate begins to band. In Fig. 6 the history of the displacement for the point in the middle of the plate is shown. At the beginning of the process, the displacement is zero until the pressure wave reaches the outer surface of the plate. Then the displacement increases rapidly and finally reaches a plateau. The simulations result for three charge -to-sample distances show a little overestimated respond.

It should be pointed out that in the case of the distance equal to 0.625m (curve FEM A3), the numerical simulation does not predict a decrease of displacement. This can be explained as an effect of adopted simplified boundary conditions, as mentioned. In [3] part d) of the model (Fig. 3) is supported by a frame - which is not included in the presented model due to lack of data. It is clear that in the experiment this frame acts as elastic support, which is initially compressed due to wave loading and after this energy is released in the opposite direction compared to the wave front. This release might be the reason that EXP

A31 and A33 finally deforms towards the charge. Such results are analogous to the one observed in [44] and [15]. In both papers, this counterintuitive or anomalous response (the permanent deflection in the direction opposite that of the load) was encountered numerically and experimentally, respectively. Similarly to the above statements the reason for such phenomenon was sought in involving acute sensitivities to the physical parameters (loading, structure geometry, and material behaviour) as well as a consequence of dynamic instabilities akin to snap-buckling.

A detailed comparison of experimentally obtained deformation profile at the centre along the x-axis for selected time instances versus numerical one for EXP A31 case is presented in Fig. 7. The comparison confirms good agreement of the obtained numerical results for the first stage of the process. However, in the second part, the difference is observed as discussed in the above paragraph. Nonetheless, we consider this initial agreement as a crucial achievement of this paper, namely not only agreement in a point (Fig. 6) is observed but the overall deformation (Fig. 7) is mapped with high precision and was possible due to plastic anisotropy, work hardening-softening effects, thermomechanical coupling and damage in the constitutive model.

In addition to the presented profiles, a full-field displacement distribution is obtained for the sample (Fig. 8). As expected, the highest values of out of plane displacements are in the centre part of the plate.

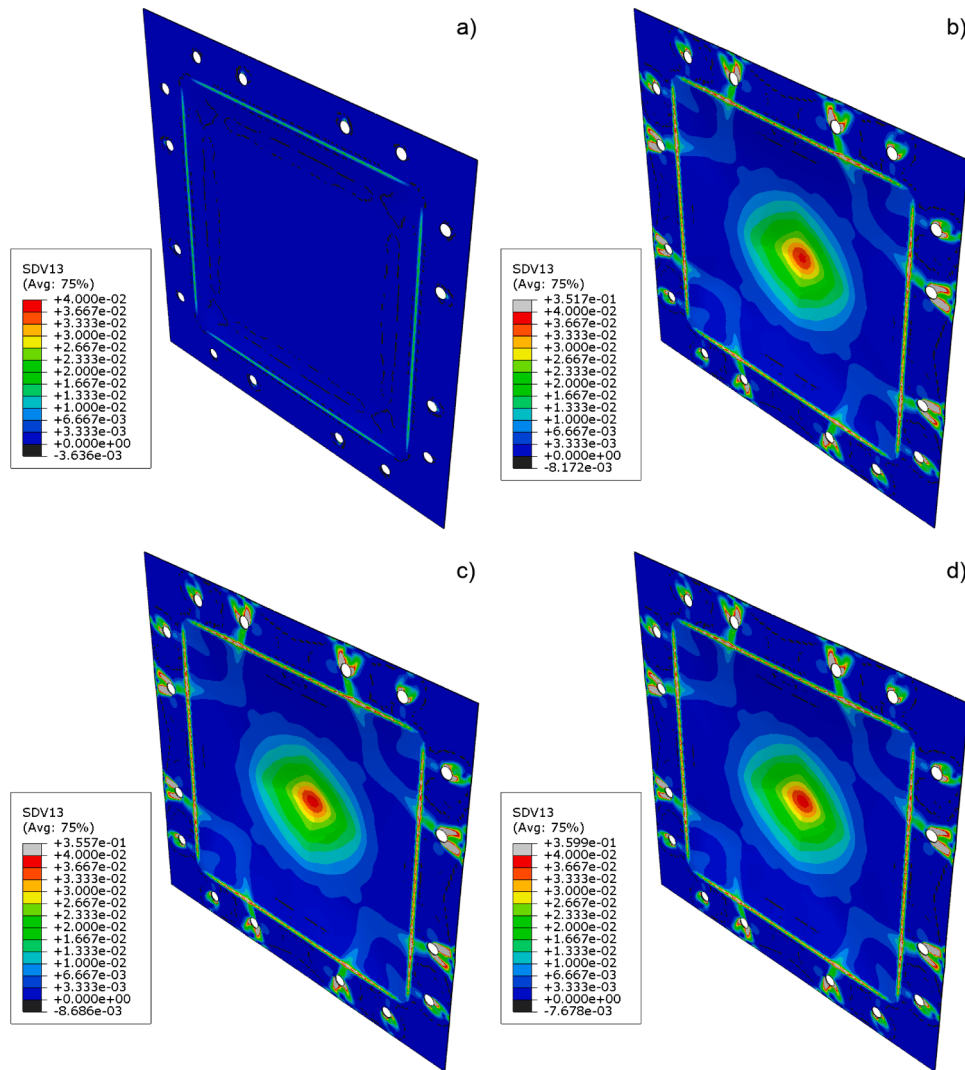


Fig. 10. Evolution of equivalent plastic strain for time instances a) 0.25ms, b) 1.25ms, c) 3.0ms and d) 6.0ms.

Moreover, the displacement distribution slightly reflects the plastic anisotropy of the material.

It is clear that numerical simulations allow having much more detailed insight into the evolution of tested material state during the blast loading compared to the available experimental techniques. With this respect, below, the selected results for FEM A3 (A31) case are discussed to point out the evolution of dynamic yield stress, equivalent plastic strain and temperature in the process time.

First, let us analyse the evolution of the initial plastic yield stress. During the deformation, on the one hand, the initial yield stress is increasing due to the increase of the plastic strain (isotropic hardening), and on the other hand, the damage growth and temperature rise cause the reduction of the yield stress (softening). In Fig. 9 the evolution of the initial plastic yield stress is shown. The process starts from homogeneous distribution of the yield stress equal to 70 MPa. Then the distribution begins to be heterogeneous with the highest values in the middle of the plate. The isotropic hardening of the material is observed. In subsequent time points, it can also be noticed that at some regions (blue colour) the yield stress is lower than the value at the beginning of the process due to the fact that plastic deformation is accompanied by the heat generation and intrinsic damage (cf. Eq. (11)).

Secondly, one of the state variables used in the material model is the equivalent plastic strain which controls the plastic behaviour of the sample. During the deformation process, the highest values of this

variable are obtained in the centre of the plate, and in the area of the support edge and near the bolt holes (Fig. 10). The plastic deformation starts with the supporting edges (Fig. 10a). Then, the plastic zone spreads out to the centre of the plate and regions around the holes for the bolts (Fig. 10b). Such distribution is maintained until the end of the process (Fig. 10d).

Finally, it should be mentioned that since the material damage parameter and temperature (due to adiabatic conditions assumption) are functions of equivalent plastic strain, their distributions are analogous to the already presented results (cf. Eqs. (10) and (12)). With this respect, the evolution of the temperature field, shown in Fig. 11, includes areas similar to zones of intensified plastic deformation (Fig. 10). The maximum temperature increase in the process is about 30 K. This means that the material softening due to temperature is a secondary effect in this process. The above statement may not always hold as presented in [7] where similar configuration but for different material and geometrical details was analysed. According to the data presented in [7] the obtained temperature increase can be as high as 500 K. Such difference in the results can be explained by the values of the equivalent plastic strain to which the temperature is proportional. In [7] these values were very large (locally up to 35), while in the presented work, the same values are a hundred times smaller (which is also caused by the damage variable in the presented formulation).

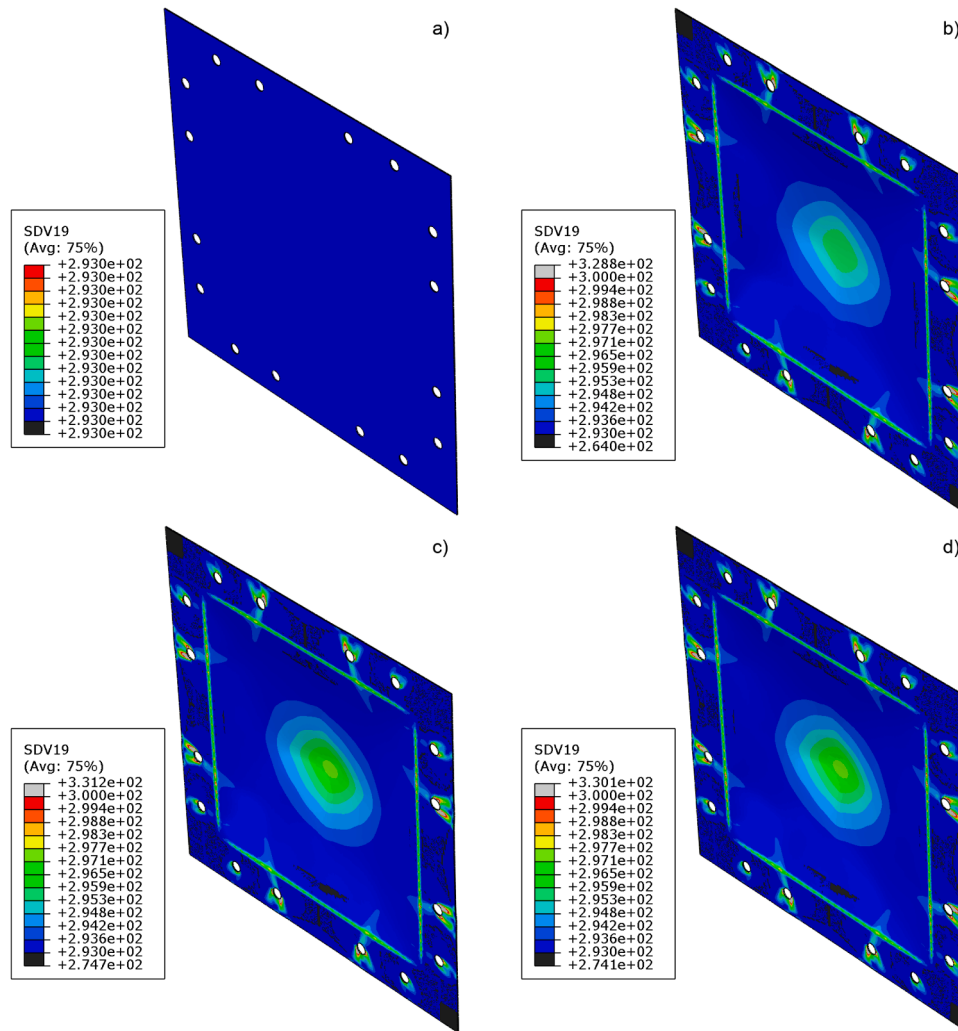


Fig. 11. Evolution of temperature for time instances a) 0.25ms, 1.25ms, c) 3.0ms and d) 6.0ms.

## 6. Conclusions

The finite element simulations in the fractional viscoplasticity framework have been successfully applied to study the deformation process of an aluminium plate under air-blast loading. The fractional viscoplastic material model for aluminium alloy EN AW 1050A-H14 was calibrated based on the experimental results of uniaxial tension tests conducted for different directions due to anisotropy. The calibrated material model was used to perform numerical simulations for three distances of the plate's air-blast loading. The finite element results were compared with those from experiments, and acceptable agreement has been obtained. Finally, it is crucial that the applied material model takes into account the plastic anisotropy, isotropic hardening and softening, rate sensitivity and implicit and explicit non-localities.

### CRedit authorship contribution statement

**Wojciech Sumelka:** Conceptualization, Formal analysis, Investigation, Writing – original draft, Writing – review & editing, Supervision, Project administration, Funding acquisition. **Marcin Nowak:** Methodology, Software, Investigation, Writing – original draft, Writing – review & editing. **Amr A. Nassr:** Methodology, Resources. **Hasan Al-Rifaie:** Methodology, Investigation. **Michał Malendowski:** Investigation. **Tomasz Gajewski:** Data curation, Visualization. **Piotr Peksa:** Validation. **Robert Studziński:** Validation, Visualization. **Piotr W. Sielicki:** Software, Writing – review & editing, Project administration, Funding

acquisition.

### Declaration of Competing Interest

The authors declare that they have no known competing financial interests or personal relationships that could have appeared to influence the work reported in this paper.

### Acknowledgements

This work is supported by the National Science Centre, Poland under Grant No. 2017/27/B/ST8/00351 and by the National Centre for Research and Development Poland under the grant DOB-BIO10/01/02/2019 in the frame of Defense and Security Programme.

### References

- [1] Abaqus. Abaqus version 6.12 collection. SIMULIA Worldwide Headquarters, Providence, RI.; 2012.
- [2] Al-Rifaie H, Sumelka W. Improving the blast resistance of large steel gates-numerical study. *Materials (Basel)* 2020;13(9).
- [3] Aune V, Fagerholt E, Hauge K, Langseth M, Børvik T. Experimental study on the response of thin aluminium and steel plates subjected to airblast loading. *Int J Impact Eng* 2016;90:106–21.
- [4] Aune V, Valsamos G, Casadei F, Langseth M, Børvik T. On the dynamic response of blast-loaded steel plates with and without pre-formed holes. *Int J Impact Eng* 2017; 108:27–46.

- [5] Børvik T, Burbach A, Langberg H, Langseth M. On the ballistic and blast load response of a 20ft iso container protected with aluminium panels filled with a local mass - phase ii: validation of protective system. *Eng Struct* 2008;30(6):1621–31.
- [6] Børvik T, Hanssen A, Dey S, Langberg H, Langseth M. On the ballistic and blast load response of a 20 ft ISO container protected with aluminium panels filled with a local mass - phase i: design of protective system. *Eng Struct* 2008;30(6):1605–20.
- [7] Chung Kim Yuen S, Nurick G. Experimental and numerical studies on the response of quadrangular stiffened plates. part i: subjected to uniform blast load. *Int J Impact Eng* 2005;31(1):55–83. <https://doi.org/10.1016/j.ijimpeng.2003.09.048>.
- [8] Clarke S, nad S, Fay SR, Barr A, Tyas A, Gant M, Elgy I. Characterisation of buried blast loading. *Proceedings of the Royal Society A: Mathematical, Physical and Engineering Sciences* 2020;476(2236).
- [9] Denny J, Clubley S. Long-duration blast loading & response of steel column sections at different angles of incidence. *Eng Struct* 2019;178:331–42.
- [10] Grimsmo E, Clausen A, Aalberg A, Langseth M. A numerical study of beam-to-column joints subjected to impact. *Eng Struct* 2016;120:103–15.
- [11] Hadianfard M, Malekpour S, Momeni M. Reliability analysis of h-section steel columns under blast loading. *Struct Saf* 2018;75:45–56.
- [12] Hanssen A, Enstock L, Langseth M. Close-range blast loading of aluminium foam panels. *Int J Impact Eng* 2002;27(6):593–618.
- [13] Kilbas A, Srivastava H, Trujillo J. Theory and applications of fractional differential equations. Amsterdam: Elsevier; 2006.
- [14] Kilbas A, Srivastava H, Trujillo J. Theory and applications of fractional differential equations. Elsevier Science & Tech; 2006.
- [15] Kolsky H, Rush P, Symonds P. Some experimental observations of anomalous response of fully clamped beams. *Int J Impact Eng* 1991;11(4):445–56.
- [16] Kuciewicz M., Baranowski P., Malachowski J.. Determination and validation of karagozian-case concrete constitutive model parameters for numerical modeling of dolomite rock. *Int J Rock Mech Min Sci*; 129(-).
- [17] Leszczyński J. An introduction to fractional mechanics. Pub. Office of Czestochowa University of Technology; 2011.
- [18] Li Y, Sun Y, Ju W. Cyclic fractional plastic model for granular soils. *Frontiers in Built Environment* 2019;5.
- [19] Longère P, Geffroy-Grèze A-G, Leblé B, Dragon A. Ship structure steel plate failure under near-field air-blast loading: numerical simulations vs experiment. *Int J Impact Eng* 2013;62:88–98.
- [20] Mainardi F. Fractional calculus and waves in linear viscoelasticity. IMPERIAL COLLEGE PRESS; 2010.
- [21] Neuberger A, Peles S, Rittel D. Springback of circular clamped armor steel plates subjected to spherical air-blast loading 2009;36(1):53–60.
- [22] Nurick G, Gelman M, Marshall N. Tearing of blast loaded plates with clamped boundary conditions. *Int J Impact Eng* 1996;18(7):803–27.
- [23] Nurick G, Martin J. Deformation of thin plates subjected to impulsive loading-a review: part i: theoretical considerations. *Int J Impact Eng* 1989;8(2):159–70.
- [24] Nurick G, Martin J. Deformation of thin plates subjected to impulsive loading-a review part ii: experimental studies. *Int J Impact Eng* 1989;8(2):171–86.
- [25] Olson M, Nurick G, Fagnan J. Deformation and rupture of blast loaded square plates-predictions and experiments. *Int J Impact Eng* 1993;13(2):279–91.
- [26] Perzyna P. The constitutive equations for rate sensitive plastic materials. *Q top Q Appl Math* 1963;20:321–32.
- [27] Podlubny I. Fractional differential equations: an introduction to fractional derivatives, fractional differential equations, to methods of their solution and some of their applications. Elsevier Science; 1998.
- [28] Podlubny I. Fractional differential equations. Mathematics in Science and Engineering, vol. 198. Academic Press; 1999.
- [29] Qu P-F, Zhu Q-Z, Sun Y-F. Elastoplastic modelling of mechanical behavior of rocks with fractional-order plastic flow. *Int J Mech Sci* 2019;163.
- [30] Remennikov A, Ngo T, Mohotti D, Uy B, Netherton M. Experimental investigation and simplified modeling of response of steel plates subjected to close-in blast loading from spherical liquid explosive charges. *Int J Impact Eng* 2017;101:78–89.
- [31] Rigby S, Tyas A, Bennett T. Elastic-plastic response of plates subjected to cleared blast loads. *Int J Impact Eng* 2014;66:37–47. <https://doi.org/10.1016/j.ijimpeng.2013.12.006>.
- [32] Sabuwala T, Linzell D, Krauthammer T. Finite element analysis of steel beam to column connections subjected to blast loads. *Int J Impact Eng* 2005;31:861–76. <https://doi.org/10.1016/j.ijimpeng.2004.04.013>.
- [33] Samko S, Kilbas AA, Marichev OI. Fractional integrals and derivatives: Theory and applications. 1993.
- [34] Sielicki PW, Pludra A, Przybylski M. Experimental measurement of the bullet trajectory after perforation of a chambered window. *Int J Appl Glass Sci* 2019;10(4):441–8.
- [35] Sielicki PW, Sumelka W, Łodygowski T. Close range explosive loading on steel column in the framework of anisotropic viscoplasticity. *Metals (Basel)* 2019;9(4): 1–19.
- [36] Sielicki PW, Łodygowski T. Masonry wall behaviour under explosive loading. *Eng Fail Anal* 2019;104:274–91.
- [37] Sielicki PW, Ślosarczyk A, Szulc D. Concrete slab fragmentation after bullet impact: an experimental study. *International Journal of Protective Structures* 2019;10(3): 380–9.
- [38] Song S, Sun Y. Flow liquefaction instability and the permissible range of fractional order of sand. *European Journal of Environmental and Civil Engineering* 2019;0(0):1–16.
- [39] Sumelka W. Fractional viscoplasticity. *Mech Res Commun* 2014;56:31–6.
- [40] Sumelka W, Nowak M. Non-normality and induced plastic anisotropy under fractional plastic flow rule: a numerical study. *Int J Numer Anal Methods Geomech* 2016;40:651–75.
- [41] Sumelka W, Nowak M. On a general numerical scheme for the fractional plastic flow rule. *Mech Mater* 2017;DOI: 10.1016/j.mechmat.2017.02.005.
- [42] Sumelka W. Application of fractional continuum mechanics to rate independent plasticity. *Acta Mech* 2014;225:3247–64.
- [43] Sun Y, Chen C. Fractional order creep model for coral sand. *Mechanics of Time-Dependent Materials* 2018.
- [44] Symonds P, Yu T. Counterintuitive behavior in a problem of elastic-plastic beam dynamics. *Journal of Applied Mechanics, Transactions ASME* 1985;52(3):517–22.
- [45] Szymczyk M, Nowak M, Sumelka W. Plastic strain localization in an extreme dynamic tension test of steel sheet in the framework of fractional viscoplasticity. *Thin-Walled Structures* 2020;149.
- [46] Szymczyk M, Nowak M, Sumelka W. Numerical study of dynamic properties of fractional viscoplasticity model. *Symmetry (Basel)* 2018;10(7).
- [47] Tarasov VE. Fractional vector calculus and fractional maxwell's equations. *Ann Phys (N Y)* 2008;323(11):2756–78.
- [48] Teeling-Smith R, Nurick G. The deformation and tearing of thin circular plates subjected to impulsive loads. *Int J Impact Eng* 1991;11(1):77–91.
- [49] W. D. P. P. Investigation of macrocrack propagation along a bimaterial interface in adiabatic dynamic processes as a problem of mesomechanics. *Engineering Transactins* 2006;54(4):289–321.
- [50] Wierzbicki T, Nurick G. Large deformation of thin plates under localised impulsive loading. *Int J Impact Eng* 1996;18(7):899–918.
- [51] Xiao R, Sun H, Chen W. A finite deformation fractional viscoplastic model for the glass transition behavior of amorphous polymers. *Int J Non Linear Mech* 2017;93: 7–14.
- [52] Zhang X, Meng Q, Bedon C, Sielicki PW. Strengthening of laminated glass windows against windborne debris impact. *International Journal of Structural Glass and Advanced Materials Research* 2020;4(1):209–24.